Rotational inertia-induced glassy transition in chiral particle systems

Bao-quan Ai,[1,2,*] Rui-xue Guo,[1,2] Chun-hua Zeng,[3,†] and Ya-feng He[4,‡]

[1]*Key Laboratory of Atomic and Subatomic Structure and Quantum Control (Ministry of Education), and School of Physics, South China Normal University, Guangzhou 510006, China*

[2]*Guangdong Provincial Key Laboratory of Quantum Engineering and Quantum Materials, and Guangdong-Hong Kong Joint Laboratory of Quantum Matter, South China Normal University, Guangzhou 510006, China*

[3]*Faculty of Science, Kunming University of Science and Technology, Kunming 650500, China*

[4]*College of Physics Science and Technology, Hebei University, Baoding 071002, China*

(Received 27 January 2024; accepted 12 May 2024; published 3 June 2024)

The dense active matter exhibits characteristics reminiscent of traditional glassy phenomena, yet the role of rotational inertia in glass dynamics remains elusive. In this study, we investigate the glass dynamics of chiral active particles influenced by rotational inertia. Rotational inertia endows exponential memory to particle orientation, restricting its alteration and amplifying the effective persistence time. At lower spinning frequencies, the diffusion coefficient exhibits a peak function relative to rotational inertia for shorter persistence times, while it steadily increases with rotational inertia for longer persistence times. In the realm of high-frequency spinning, the impact of rotational inertia on diffusion behavior becomes more pronounced, resulting in a nonmonotonic and intricate relationship between the diffusion coefficient and rotational inertia. Consequently, the introduction of rotational inertia significantly alters the glassy dynamics of chiral active particles, allowing for the control over transitions between fluid and glassy states by modulating rotational inertia. Moreover, our findings indicate that at a specific spinning temperature, there exists an optimal spinning frequency at which the diffusion coefficient attains its maximum value.

DOI: 10.1103/PhysRevE.109.064902

I. INTRODUCTION

Glasses, recognized as disordered solids with slow relaxation dynamics [1,2], have been extensively studied for decades. In the past decade, it has become increasingly apparent that phenomena associated with glassy dynamics are also observable in dense active matter systems. Active forces driving particle systems out of equilibrium have recently been identified as key contributors to nonequilibrium glass transitions, representing a novel form of dynamic arrest [1]. The manifestations of this slow dynamics, resembling supercooled fluids approaching an equilibrium glass transition, include phenomena such as caging, dynamical slowing down, nonexponential time correlation functions, and dynamic heterogeneity [2]. Remarkably, by increasing the density to large values, self-propelled systems can reach a dynamically arrested or glassy state, known as active glassy states, which exhibit remarkable similarities to conventional passive ones [3]. Observations of this phenomenon have been notably reported in living cells and cell layers [4–6], synthetic colloidal assemblies [7], granular matter [8], and various simulations and theoretical studies [9–28]. The research efforts in comprehensively understanding active glassy states and their relation to conventional passive counterparts have rapidly gained momentum, situated at the intersection of the broader fields of active matter and glassy physics.

The existence of chirality in chiral active systems can yield intriguing dynamic behaviors [29–33]. Examples of these fascinating phenomena include active microrheology, the Hall effect, and jamming within chiral fluids [29], as well as odd diffusivity observed in chiral random motion [30], and the nonreciprocal response of a two-dimensional fluid exhibiting odd viscosity [31]. Debets and colleagues [33] recently mapped out glassy dynamics in chiral fluids, unveiling a complex dynamic behavior when the chiral fluid meets glassy conditions, compared to a standard linear active fluid like ordinary active Brownian particles. These dynamics were found to be overdamped, however, for macroscopic or microparticles moving in a gas, inertial effects come into play, rendering the dynamics underdamped. Rotational inertia, specifically, has been discerned in recent studies to significantly steer the system's dynamics, for instance, boosting the correlation length of the spatial velocity correlations within the dense cluster [34–38]. The appearance of collective phenomena like motility-induced phase separation and spatial velocity correlations are strong indications of an increase in rotational persistence which is enhanced by rotational inertia [38]. The influence of rotational inertia on nonequilibrium glass dynamics of chiral active matter is an unsolved mystery that begs exploration, thereby making our research on chiral active matter's glass dynamics influenced by rotational inertia.

In this study, we aim to address this pivotal question related to a chiral active system with rotational inertia. Rotational

*aibq@scnu.edu.cn
†zchh2009@126.com
‡heyf@hbu.edu.cn

 ©2024 American Physical Society

inertia provides an exponential memory to the particle orientation, hindering its change and prolonging the effective persistence time. The interplay between rotational inertia and the particle persistence enriches the dynamics of the system. When rotational inertia governs the dynamics during high-frequency spinning, a continuous increase in rotational inertia causes the diffusion coefficient to initially rise from an extremely small value to a peak, then to plummet to a trough, ascend to another peak, and ultimately tend towards zero. In contrast, for lower-frequency spinning scenarios, the diffusion coefficient is peaked function of rotational inertia for small persistence time and increases with rotational inertia for large persistence time. Hence, by manipulating rotational inertia, one can facilitate transitions, even multiple transitions-between the fluid and glassy states in the system. Given a constant spinning temperature, there is an appropriate spinning frequency at which the diffusion coefficient reaches its maximum. Our findings are essential for understanding the glassy dynamics of chiral active matter with rotational inertia and can be applied to future experiments aiming to observe this nontrivial dynamics.

II. MODEL AND METHODS

We consider a two-dimensional Kob-Andersen mixture, which comprises self-propelled particles A, B in the ratio 65 : 35. These particles are accommodated within a two-dimensional box of size $L \times L$, operating under periodic boundary conditions. Each particle's dynamics are defined by the position of its center $\mathbf{r}_i \equiv (x_i, y_i)$ and the orientation of its polar axis $\mathbf{n}_i \equiv (\cos\theta_i(t), \sin\theta_i(t))$, denoted as $\theta_i(t)$. The dynamics of particle i comply with the overdamped Langevin equation,

$$\frac{d\mathbf{r}_i}{dt} = v_0\mathbf{n}_i + \mu\mathbf{F}_i + \sqrt{2D_0}\boldsymbol{\zeta}_i(t), \tag{1}$$

where v_0 represents the self-propulsion speed and μ denotes the mobility,

$$J\frac{d^2\theta_i}{dt^2} = -\gamma_r\frac{d\theta_i}{dt} + \omega + \gamma_r\sqrt{2D_r}\xi_i(t), \tag{2}$$

where J is rotational inertia and γ_r is the rotational friction coefficient. The constants D_0 and D_r represent the translational and rotational diffusion coefficients, respectively. $\boldsymbol{\zeta}_i(t)$ and $\xi_i(t)$ are unit-variance Gaussian white-noise random numbers with zero average. In most cases, we disregard translational inertia primarily because our main focus is on studying the impact of rotational inertia on the dynamics of spinning particle systems. Additionally, in certain scenarios, such as when the particle is characterized by a small mass and large volume, translational inertia becomes insignificant. ω is the spinning frequency. We can define a spinning temperature [33] $T_\omega = v_0^2/2\omega$, which represents a measure for the amount of energy that is dissipated by a single particle during on circle motion. We define the persistent time of a single-trajectory $\tau_p = 1/D_r$, the typical rotational inertial time $\tau_r = J/\gamma_r$, and the spinning period $\tau_\omega = 2\pi/\omega$.

The term $\mathbf{F}_i$ represents the force contribution due to steric interactions between particles. This interaction force is given by $\mathbf{F}_i = -\sum_{j\neq i}\nabla_i V_{\alpha\beta}(r_{ij})$, derived from a quasihard sphere power law potential [33,39] $V_{\alpha\beta}(r) = 4\epsilon_{\alpha\beta}(\frac{\sigma_{\alpha\beta}}{r})^{36}$. The interaction parameters are as follows: $\epsilon_{\mathrm{AA}} = 1$, $\epsilon_{\mathrm{AB}} = 1.5$, $\epsilon_{\mathrm{BB}} = 0.5$, $\sigma_{\mathrm{AA}} = 1$, $\sigma_{\mathrm{AB}} = 0.8$, and $\sigma_{\mathrm{BB}} = 0.88$. Here we select parameters typical of the standard Kob-Andersen mixture, which facilitates the simulation of glassy states and glass transitions. The inclusion of particles with different sizes aims to prevent crystallization of the system at low temperatures and high densities. We utilize reduced units, where σ_{AA}, ϵ_{AA}, $\epsilon_{\mathrm{AA}}/k_B$, $\sigma_{\mathrm{AA}}^2/\mu\epsilon_{\mathrm{AA}}$ denote the units of length, energy, temperature, and time, respectively.

To investigate the dynamic behavior of the system, we define the time-dependent mean-square displacement (MSD) as follows:

$$\langle\Delta r^2(t)\rangle = \langle|\mathbf{r}_i(t) - \mathbf{r}_i(0)|^2\rangle, \tag{3}$$

where the brackets indicate an ensemble average performed under steady-state conditions. We obtain the longtime diffusion coefficient D_L by assuming the longtime behavior as $D_L = \lim_{t\to\infty}\frac{\langle\Delta r^2(t)\rangle}{4t}$.

To better understand the glassy dynamics of our model, we also calculate the self-intermediate scattering function $F_s(k_m, t) = \langle e^{-i\mathbf{k}\cdot\mathbf{r}_j(0)}e^{i\mathbf{k}\cdot\mathbf{r}_j(t)}\rangle$, where the wave number k_m corresponds to the main peak of the structure factor. The self-intermediate scattering function represents the probability distribution of finding a particle at a certain position after a time delay t, given its initial position. By analyzing the decay of $F_s(k_m, t)$ over time, we can extract valuable information about the structural relaxation, diffusion processes, and collective motion of particles in various materials.

Dynamical heterogeneity is a notable characteristic of glass systems. We typically utilize non-Gaussian parameter analysis to examine the heterogeneity of supercooled liquid dynamics. In two dimensions, it is defined as [40,41]

$$\alpha_2(t) = \frac{\langle\Delta r^4(t)\rangle}{2\langle\Delta r^2(t)\rangle^2} - 1. \tag{4}$$

If the particles undergo normal homogeneous diffusion, then the displacement distributions are Gaussian such that $\alpha_2(t) = 0$. If the distributions reveal tails and are much wider than expected for a Gaussian distribution, then $\alpha_2(t) > 0$, indicating that the system is dynamically heterogeneous. Conversely, $\alpha_2(t) < 0$ generally indicates that a population of particles performs cooperative directional motion.

It should be noted that in the case of dynamically arrested states, diffusion coefficients cannot be well computed as the particle motion in the system is not purely diffusive. However, the effective diffusion behavior of particles in these states can still be depicted using the long-time diffusion constant. The long-time diffusion constant D_L, combined with MSD, the self-intermediate scattering function, and the non-Gaussian parameter, is a common rule-of-thumb in the field for determining whether the system is in a glassy or dynamically arrested state [16,33]. In our study, we observed that if D_L falls below 10^{-4}, it serves as an indicator that the system operates in a glassy or dynamically arrested state. To describe the density of particles in the box, we use the particle number density $\rho = N/L^2$. Here we fixed $\rho = 1.2$, which is in the regime where the system shows dynamical arrest at low temperatures.

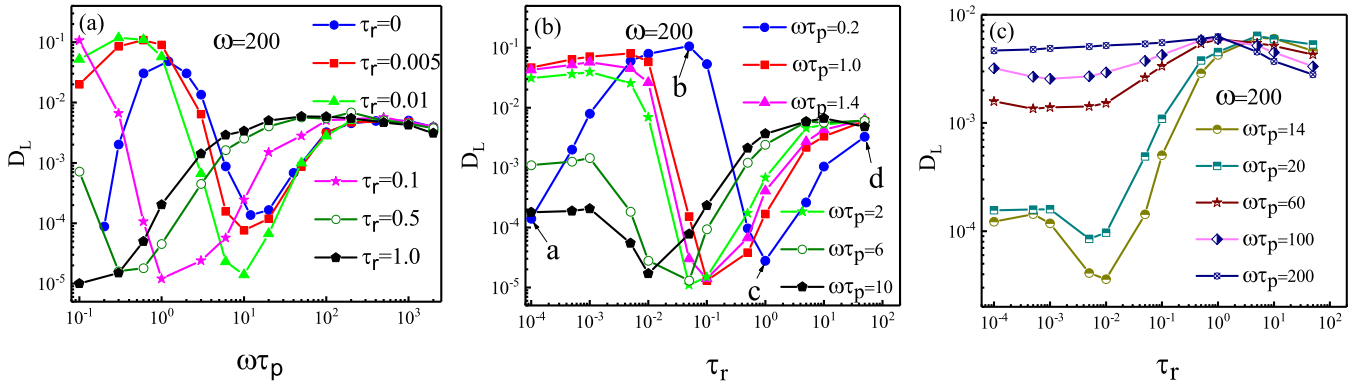

FIG. 1. The longtime diffusion coefficient D_L (a) as a function of $\omega\tau_p$ for different τ_r and (b, c) as a function of τ_r for different $\omega\tau_p$.

Equations (1) and (2) are integrated utilizing the stochastic Euler algorithm. The integration time step is chosen to be 10^{-4} and the total integration time is 10^5. The system is operated for a substantial duration, typically between 500 and 10^4, to prevent any aging effects, after which the tracking of the particles is carried out over time. We considered 50 realizations to improve the accuracy and minimize statistical errors. For every simulation run, particle positions are initialized using a uniform random distribution within the box, and orientations are randomly chosen over the interval $[0, 2\pi]$. Unless otherwise specified, our simulations utilize the following parameter sets: $\mu = 1$, $\gamma_r = 1.0$, and $N = 1000$. We set $T_\omega = 4$, ensuring that the system exhibits moderately supercooled behavior. The presented results have shown robustness when these parameters are reasonably altered.

III. RESULTS AND DISCUSSION

Initially, we evaluate the situation in which self-propulsion overwhelmingly surpasses thermal fluctuations, thus permitting us to disregard translational diffusion ($D_0 = 0$). In this case, we discuss the influence of the moment of inertia on the diffusion behavior of particles in the absence of interaction between them. For small rotational inertia, the longtime diffusion coefficient of chiral active particles asymptotically approaches [34,36,37]

$$D_L = \frac{v_0^2 D_r}{2\left(D_r^2 + \omega^2\right)}\left(1 + \frac{D_r}{\gamma_r} J\right) + O(J^2), \tag{5}$$

which predominantly grows in proportion to J. The asymptotic behavior of the longtime diffusion coefficient for large rotational inertia is [34,36,37]

$$D_L \sim \begin{cases} v_0^2 \sqrt{\frac{\pi}{8 D_r \gamma_r}}\sqrt{J} & \omega = 0, \\ 0 & \omega \neq 0. \end{cases} \tag{6}$$

When $\omega \neq 0$, D_L asymptotically approaches zero due to the impediment of diffusion by systematic circular motion. This occurrence is due to the substantial moment of inertia that confines the particle to a circular path. In contrast, when $\omega = 0$, the diffusion coefficient exhibits a monotonic increase with the growth of the moment of inertia. Therefore, for $\omega \neq 0$, the diffusion behavior displays nonmonotonic alterations as J increases.

Rotational inertia provides an exponential memory to the particle orientation, hindering its change and, in first approximation, increasing the effective persistence time, $\tau_p \to \tau_p^*$, from the overdamped value τ_p to a larger value depending on J/γ_r. Following Ref. [36], the analytical expression for τ_p^* can be calculated as

$$\tau_p^* \sim \begin{cases} \tau_p + \tau_r & \tau_r \ll \tau_p, \\ \tau_p \sqrt{\tau_r} & \tau_r \gg \tau_p. \end{cases} \tag{7}$$

Rotational inertia plays a crucial role in the complex dynamics of chiral particles. Therefore, it is of considerable interest to investigate its impact on the glass dynamics of interacting chiral Brownian particles. According to Ref. [33], the dynamics can be divided into three regimes in terms of the effective persistence time τ_p^*. (I) In the small persistence regime, where the local environment of particles primarily acts as an effective confining potential. (II) In the intermediate persistence regime where the hammering mechanism plays a crucial role. The hammering mechanism refers to the expectation that, for a sufficiently long duration and spinning frequency, particles will undergo prolonged periods of uninterrupted back-and-forth motion inside their cage, systematically colliding with the same particle. Following repeated collisions, the cage of a particle is sufficiently remodeled, allowing the particle to break out and migrate through the system. (III) In the large persistence regime, in which collective motion dominates the dynamics.

Next, we will concentrate on two prototypical scenarios: (1) High-frequency spinning ($\omega = 200$) and the spinning radius ($R = v_0/\omega = 0.2$) is less than the particle radius; (2) Low-frequency spinning ($\omega = 10$) and the spin radius ($R = 0.89$) is larger than the particle radius. In the subsequent analysis, we will concentrate on investigating the impact of rotational inertia on the glassy dynamics, by varying rotational inertial time (τ_r), the persistence time (τ_p), and the spinning frequency (ω).

Initially, we will assess the scenario where ω is set to 200, signifying a case distinguished by an especially pronounced resonant effect. Figure 1(a) delineates the longtime diffusion coefficient D_L as a function of $\omega\tau_p$ under varying τ_r parameters. In scenarios where rotational inertia is absent ($\tau_r = 0$), the obtained curve exhibits two peaks along with a valley, reminiscent of the findings of Ref. [33] and highlighting the complex dynamics. With the introduction of rotational iner-

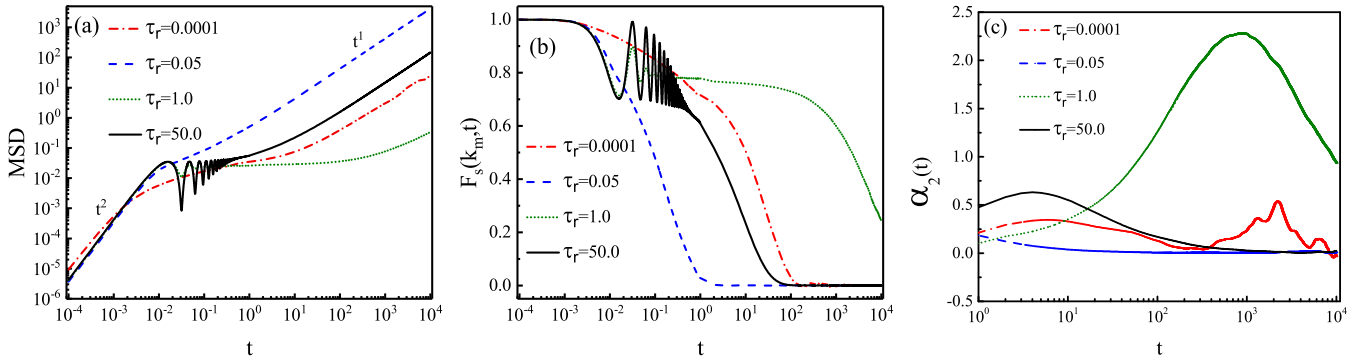

FIG. 2. (a) Mean-square displacement as a function of time t for different τ_r. (b) The self-intermediate scattering function of the majority A species as a function of t for different τ_r. (c) The non-Gaussian parameter as a function of time t for different τ_r. The height of the peak in $\alpha_2(t)$ is an indicator for dynamical heterogeneity, while a value of zero corresponds to diffusive motion. Here, $\tau_r = 0.0001, 0.05, 1.0, 50.0$ correspond to points a, b, c, d in Fig. 1(b), respectively. The other parameters are $\omega\tau_p = 0.2$ and $\omega = 200$.

tia, significant changes are observed in the system dynamics. As τ_r progresses from zero, the location of the first peak shifts towards smaller $\omega\tau_p$ values. This phenomenon can be attributed to the fact that, in the small persistence regime, particles localized in the vicinity can mimic a harmonic trap, with the peak position materializing near $\omega\tau_p^* = 1$. Note that the position of this peak and its corresponding explanation were provided in previous work [33] with $\tau_r = 0$. For a fixed value of τ_p^*, it is apparent from Eq. (7) that an increase in τ_r results in a decrease of τ_p. Consequently, the peak position shifts towards smaller $\omega\tau_p$ values. Analogously, the valley position also undergoes a similar shift. In the large persistence regime $\tau_p \gg \tau_r$ (i.e., $\omega\tau_p > 100$), Eq. (5) infers that the contribution of rotational inertia to diffusion is negligible, effectively rendering rotational inertia inconsequential to particle diffusion.

The longtime diffusion coefficient D_L versus τ_r is demonstrated in Figs. 1(b) and 1(c) for various $\omega\tau_p$. First, we examine the case of the small persistence (e.g., $\omega\tau_p = 0.2$), where two peaks and a valley are noted on the curve, mirroring the relationship between D_L and $\omega\tau_p$ at $\tau_r = 0$ as shown in Fig. 1(a). When τ_r increases from zero, D_L initially rises to its apex, then decreases to its nadir, before steadily climbing again, ultimately approaching zero. This is explicated as follows. In a situation where τ_r is very small, with $\tau_p^* < \tau_\omega$, the nearest-neighbor distance appears entirely arbitrary, i.e., the particle undergoes random collisions with all neighbors. Here, the local environment chiefly functions as an effective confinement potential, leading to the generation of the first peak. Conversely, when $\tau_p^* > \tau_\omega$, particles are likely to undertake full circular or elliptical motion within their cages, leading to a decrease in D_L. Importantly, D_L reaches its minimal value at approximately $\tau_p^* \sim 2\tau_\omega$. When $\tau_p^* > 2\tau_\omega$, repeated collisions sufficiently remodel the particle's cage, enabling the particle to break out and permeate the material, hence an increase in D_L once more, reaching its zenith. Finally, when $\tau_p^* \gg \tau_\omega$, the nearest-neighbor distance becomes very periodic, indicating that the particle collides, moves away, then collides again and so on. Remarkably, in the case of high spinning frequencies (e.g., $\omega = 200$), D_L tends towards zero and displays an absorbing state [33,42].

The dynamic activities at characteristic points a, b, c, and d on the curve are detailed in Fig. 2. We observed that at points a and c, the relaxation time of $F_s(k_m, t)$ is long and the MSD widens over time, resulting in a plateau. The presence of high peaks in the non-Gaussian parameter indicates significant heterogeneity within the system. These observations suggests that the system behaves as a frozen system, similar to glass. Contrastingly, at points b and d, the relaxation time of $F_s(k_m, t)$ is short, the MSD scales linearly over time, and the peak in $\alpha_2(t)$ disappears, suggesting a diffusive system similar to fluid. Therefore, it is possible to interchange between the fluid and glass state by adjusting rotational inertia. An observable oscillation is noticeable in both the MSD and $F_s(k_m, t)$ for the case of $\tau_r = 50$. In this case, $\tau_p^* > 2\tau_\omega$, particles progress from ballistic motion to performing a full circular or elliptical motion within their cages. This movement pattern triggers a time-dependent oscillation in the MSD. Following subsequent repeated collisions that significantly alter the structure of these cages, the particles are able to escape, leading to a linear increase in the MSD over time.

As $\omega\tau_p$ progressively increases, the positions of both the first peak and the valley shift towards smaller τ_r. This shift occurs because an increase in τ_p, under a fixed value of τ_p^*, subsequently results in a decrease in τ_r. When $\omega\tau_p$ is exceptionally high (e.g., $\omega\tau_p = 200$) shown in Fig. 1(c), the

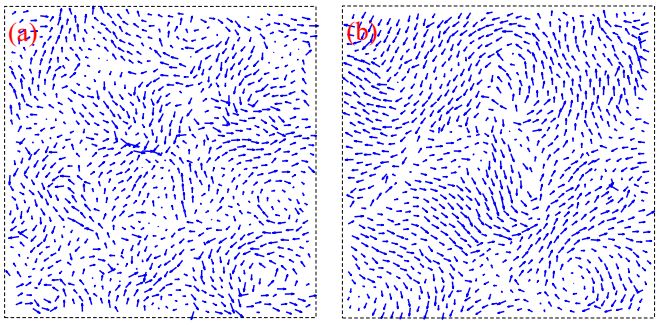

FIG. 3. Example velocity fields of chiral active particles at $\omega\tau_p = 200$. (a) $\tau_r = 0.0001$. (b) $\tau_r = 50$. In both cases, the motion can be observed to transition into a collective, vortexlike pattern.

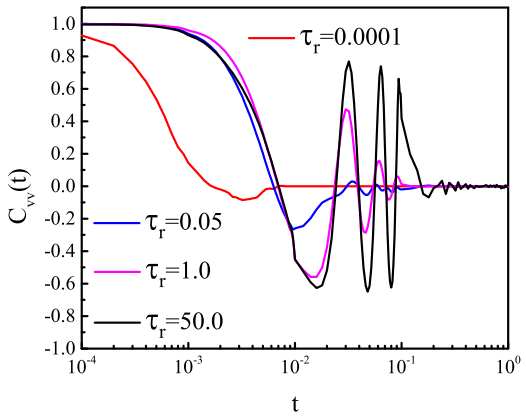

FIG. 4. The velocity autocorrelation function $C_{vv}(t)$ as a function of time t for different τ_r at $\omega\tau_p = 0.2$ and $\omega = 200$. Our observations reveal the emergence of oscillations, corresponding to a more pronounced circular particle motion inside the cage. This tendency becomes particularly evident when τ_r is increased.

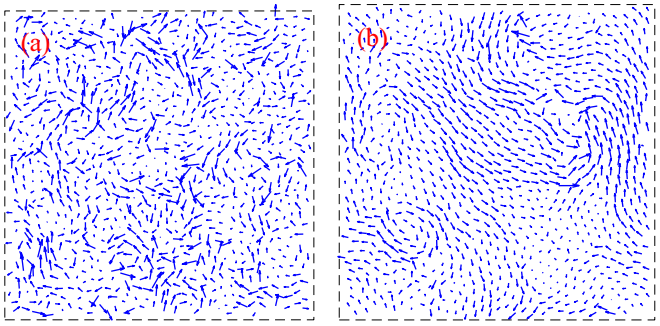

FIG. 6. Example velocity fields of chiral active particles at $\omega = 10$ and $\tau_r = 0$. (a) $\omega\tau_p = 0.1$. (b) $\omega\tau_p = 100$. The motion can be seen to become more collective and vortexlike at $\omega\tau_p = 100$.

dynamics of the system are dominated by the collective motion of particles. The velocity fields depicted in Figs. 3(a) and 3(b) demonstrate that the motion becomes collective and vortexlike at $\omega\tau_p = 200$. In particular, if τ_p significantly exceeds τ_r, the influence of the moment of inertia on the system's dynamics becomes negligible, causing both the first peak and the valley to disappear. Notably, when $\tau_r < 1$, D_L seems to remain independent of τ_r. While it is not illustrated in the figure, it should be specified that D_L approaches 0 when τ_r tends toward infinity. Within systems of nonchiral particles, the stringlike cooperative motion can be observed at temperatures well above the glass transition [43,44]. In this case, a void takes the form of a quasivoid consisting of a few neighboring free volumes and is transported by the stringlike motions it induces. However, in our system of chiral particles, this stringlike cooperative motion is difficult to observe in the glass phase due to the rapid rotation of particles. What is discernible within our system is a collective swirlinglike motion. In an attempt to quantify this collective swirlinglike motion, we have examined the normalized velocity autocorrelation function, represented as $C_{vv}(t) = \langle \dot{\mathbf{r}}_i(0)\dot{\mathbf{r}}_i(t)\rangle / \langle \dot{\mathbf{r}}_i^2 \rangle$. The normalized velocity autocorrelation function $C_{vv}(t)$ for characteristic points a, b, c, and d in Fig. 1(b) is plotted in Fig. 4. In alignment with the increasingly circular trajectories, we notice the emergence of oscillations. Moreover, the lifespan of these oscillations extends as τ_r.

Next, we discuss the glassy dynamics under conditions of low-frequency spinning (e.g., $\omega = 10$). Figure 5(a) presents D_L as a function of $\omega\tau_p$ for different τ_r. For $\tau_r = 0$, D_L monotonically increases with $\omega\tau_p$, and in the intermediate region, there is a plateau. For extremely small values of $\omega\tau_p$, the particle movement is noncollective and random [shown in Fig. 6(a)]. In the intermediate persistence regime, the valley disappears. This is because the hammering effect is weak at low frequency. In this case, the spin radius ($R = 0.89$) is larger than the particle radius. Therefore, particles seldom periodically collide with the surrounding particles in their cage (the hammering effect), but rather predominantly drive the surrounding particles to rotate together (vortexlike motion). The former inhibits diffusion, while the latter promotes diffusion. These two factors compete with each other. In the intermediate region, they are evenly matched, leading to a plateau appears in the curve. When $\omega\tau_p > 100$, vortexlike motion completely occupies the system's dynamics, thus the diffusivity increases significantly. Compared with an absorbing state caused by collective motion (large $\omega\tau_p$) at high-frequency spinning (e.g., $\omega = 200$), the collective motion here leads to an active state. The diffusivity increases significantly when $\omega\tau_p > 100$, because the particle motion becomes more collective and vortexlike [shown in Fig. 6(b)] when ω is small

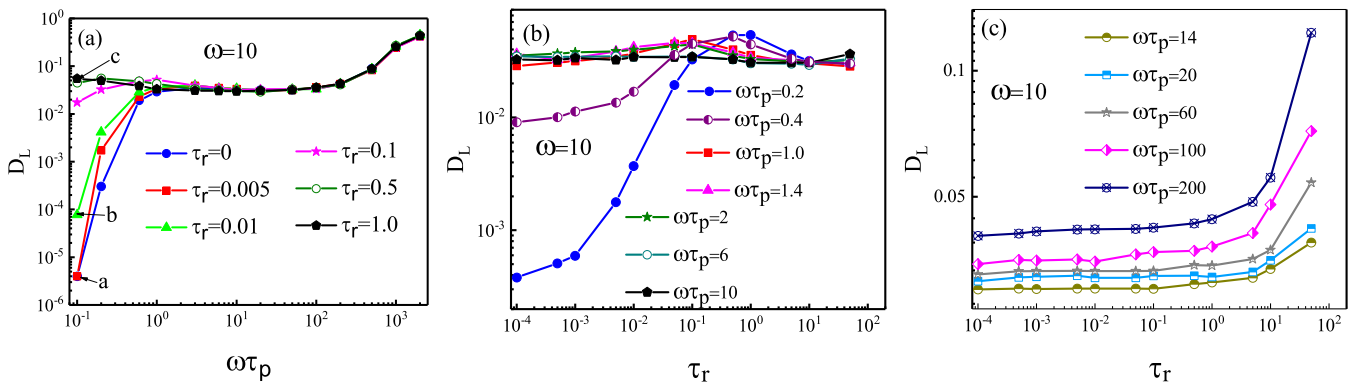

FIG. 5. The longtime diffusion coefficient D_L (a) as a function of $\omega\tau_p$ for different τ_r and (b, c) as a function of τ_r for different $\omega\tau_p$.

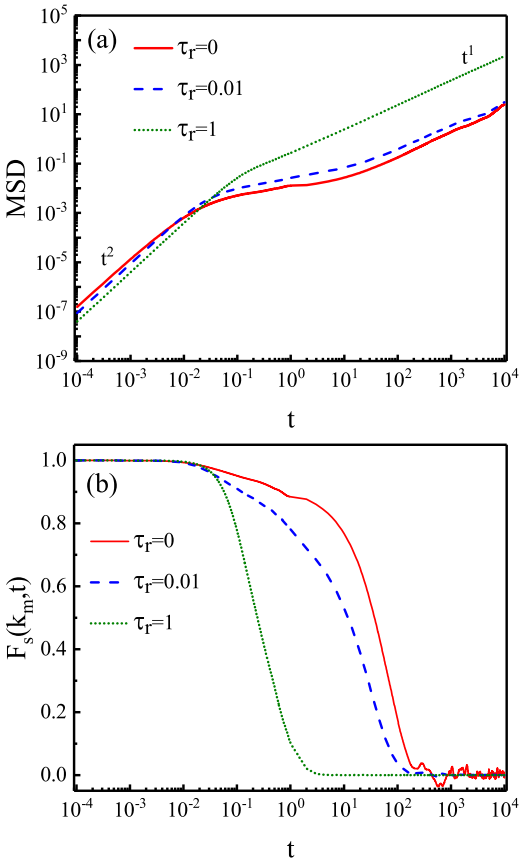

FIG. 7. (a) Mean-square displacement as a function of time t for different τ_r. (b) The self-intermediate scattering function of the majority A species as a function of t for different τ_r. Here, $\tau_r = 0, 0.01, 1$, correspond to points a, b, c in Fig. 5(a), respectively. The other parameters are $\omega\tau_p = 0.1$ and $\omega = 10$.

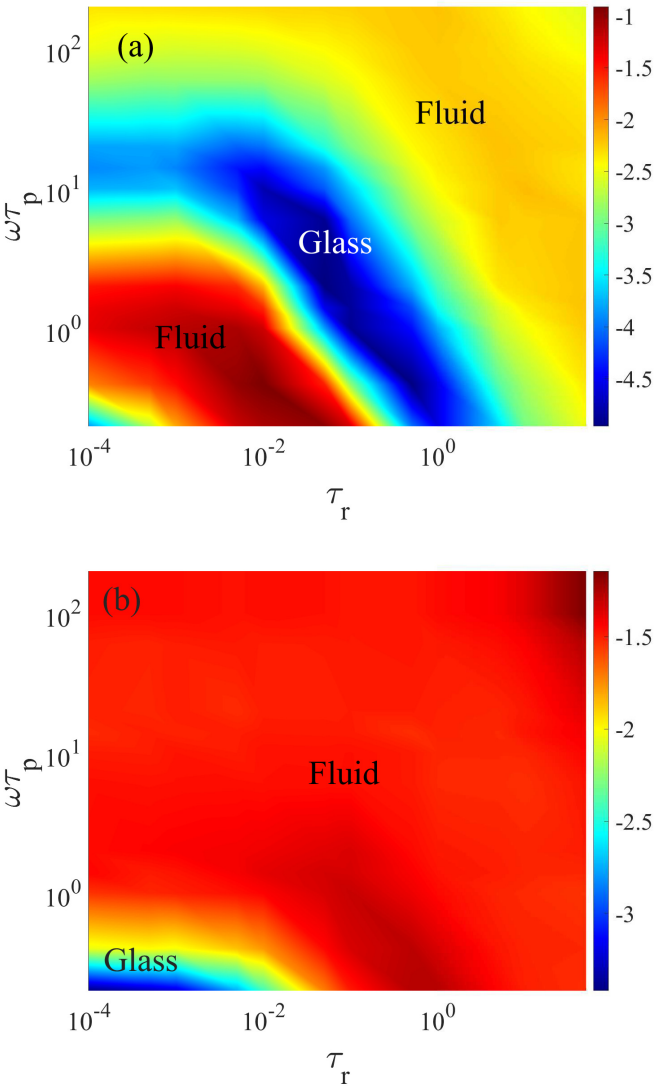

FIG. 8. Phase diagram of the longtime diffusion coefficient D_L in the $\tau_r - \omega\tau_p$ representation. (a) $\omega = 200$. (b) $\omega = 10$. The background represents the value of $\log_{10} D_L$ according to the color bar on the right.

enough and τ_p is large enough. A more detailed discussion refers to Ref. [33].

When $\omega\tau_p > 1$, rotational inertia exerts minimal influence on the diffusion behavior of particles. Conversely, when $\omega\tau_p$ is notably low, rotational inertia significantly impacts particle dynamics. Curves in Fig. 7 shows this dynamics corresponding to points a, b, c in Fig. 5(a). The relaxation time of $F_s(k_m, t)$ elongates, and the MSD broadens over time, leading to the formation of the plateau at point a ($\tau_r = 0$). This suggests the resemblance to a frozen system. Contrarily, at the point c ($\tau_r = 1.0$), the relaxation time of $F_s(k_m, t)$ is short, and the MSD exhibits a linear increase over time, implying a diffusion system akin to a fluid.

Figures 5(b) and 5(c) illustrate D_L as a function of τ_r for various $\omega\tau_p$ values, respectively. For lower $\omega\tau_p$, D_L is a peaked function of τ_r. However, as $\omega\tau_p$ increases, the curve's peaks gradually disappear, resulting in D_L becoming a monotonically increasing function of τ_r. Notably, distinct from the high-frequency scenario ($\omega = 200$) where the diffusion coefficient approaches zero when τ_r is exceedingly large, the diffusion coefficient notably increases under low frequencies ($\omega = 10$). This increase is attributed to the existence of a transition from what is termed as an "active" to an "absorbing" state when $\tau_p^* \to \infty$ upon increasing ω, as described in Refs. [33,42].

The dynamics behavior of system can be demonstrated clearly in a phase diagram as shown in Fig. 8. We designate the parameter region with $D_L < 10^{-4}$ as the glass region, where the dynamically arrested state is evidenced by a long relaxation time for $F_s(k_m, t)$ and a lengthened plateau in MSD over time. We find that the system exhibits a greater complexity under high frequency conditions [Figs. 8(a)]. In the scenario of high frequency, the system attains a glassy state (illustrated by the blue region) when both τ_r and $\omega\tau_p$ are significantly small or moderate values. In contrast, under low-frequency conditions, the system only transitions to a glassy state when both τ_r and $\omega\tau_p$ are notably small. Therefore, it is compellingly evident that the transformation from fluid to glassy states can be achieved by manipulating rotational inertia.

Figure 9 illustrates D_L as a function of ω for several circumstances. Observations reveal an optimal ω at which D_L reaches its maximum in all instances. Here, the spinning

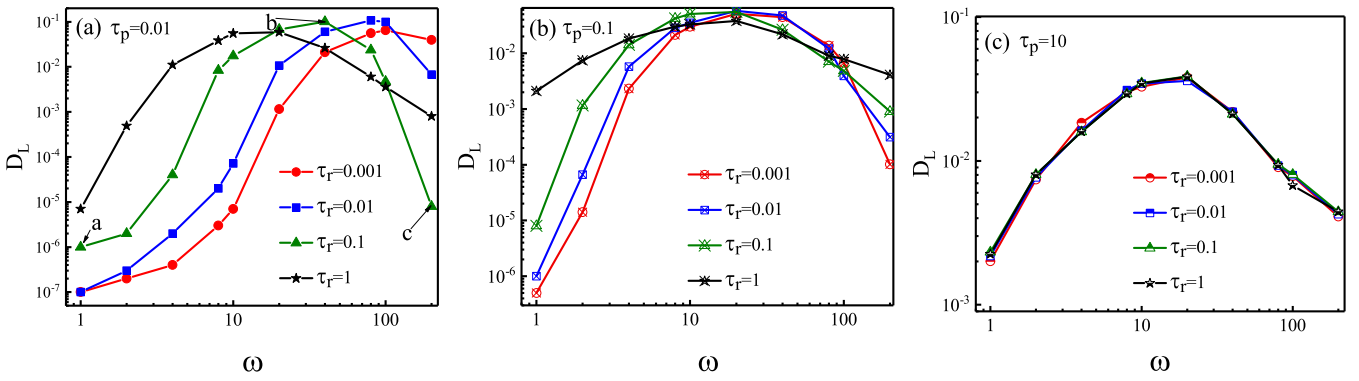

FIG. 9. The longtime diffusion coefficient D_L as a function of ω for different τ_r at (a) $\tau_p = 0.01$, (b) $\tau_p = 0.1$, and (c) $\tau_p = 10$.

temperature $T_\omega = v_0^2/\omega$ in our study is fixed at 4.0, meaning the self-propulsion speed v_0 correlates with ω. When ω approaches 0, v_0 also tends to zero, thus the self-propulsion is removed. In this instance, as we have neglected translational diffusion, the longtime diffusion coefficient tends to zero. Alternatively, as ω approaches infinity, the self-propulsion speed increases significantly. However, due to the exceedingly rapid rotations, the particles barely move, leading to an extremely low diffusion coefficient. Therefore, D_L is a peaked function of ω. Consistent behavior is observed in other variables such as the MSD, the self-intermediate scattering function, and the non-Gaussian parameter, for instance, with $\tau_r = 1.0$ as shown in Fig. 9(a). Figures 10(a), 10(b), and 10(c) reveal that at $\omega = 200$, the relaxation time of $F_s(k_m, t)$ is prolonged, the MSD increases over time, and a high peak appears in the non-Gaussian parameter. These observations suggest a system akin to a frozen state. However, at $\omega = 40$, the relaxation time of $F_s(k_m, t)$ becomes brief, the MSD scales linearly with time, and the peak in $\alpha_2(t)$ vanishes, indicative of a system undergoing fluidlike diffusion. Therefore, by adjusting the spinning frequency ω, we can manipulate the transition between the fluid and glass state.

We have also probed the effect of rotational inertia on the $D_L - \omega$ relationship for different τ_p. In certain situations where τ_p is exceptionally high (e.g., $\tau_p = 10$), as shown in Fig. 9(c), the dynamics are dominated by τ_p, resulting in a negligible impact from rotational inertia on the $D_L - \omega$ association, as evidenced by the overlap of all curves. This is because when $\tau_p \gg \tau_r$, the dynamic contribution emanating from rotational inertia can be dismissed, according to Eq. (7). When τ_p is moderate (e.g., $\tau_p = 0.1$), the persistence from self-propulsion competes with the persistence from rotational inertia. Rotational inertia predominates at low and high frequencies, whereas self-propulsion is more pronounced at intermediate frequencies. As a result, rotational inertia does not significantly affect diffusion at intermediate frequencies but profoundly influences it at low and high frequencies. Specifically, the diffusion coefficient sees an increment with the rise in rotational inertia at both these frequencies. Consequently, an increase in rotational inertia flattens the curve and makes the peak characteristics less accentuated. However, where τ_p is remarkably small (e.g., $\tau_p = 0.01$), the dynamics are heavily influenced by rotational inertia, resulting in a significant effect on the $D_L - \omega$ relationship. In such cases, an increase in rotational inertia shifts the peak of the curve towards the lower frequencies.

Figure 11 illustrates a comparison of the diffusion behavior of particles with and without chirality. For nonspinning particles, the diffusion coefficient, D_L, increases monotonically with the persistence time, τ_p. Alternatively, spinning particles demonstrate a nonmonotonic relationship between D_L and τ_p. The impact of chirality on glass dynamics can be categorized into three phases based on the competition between the effective persistence time, τ^*, and the spin period, τ_ω. In

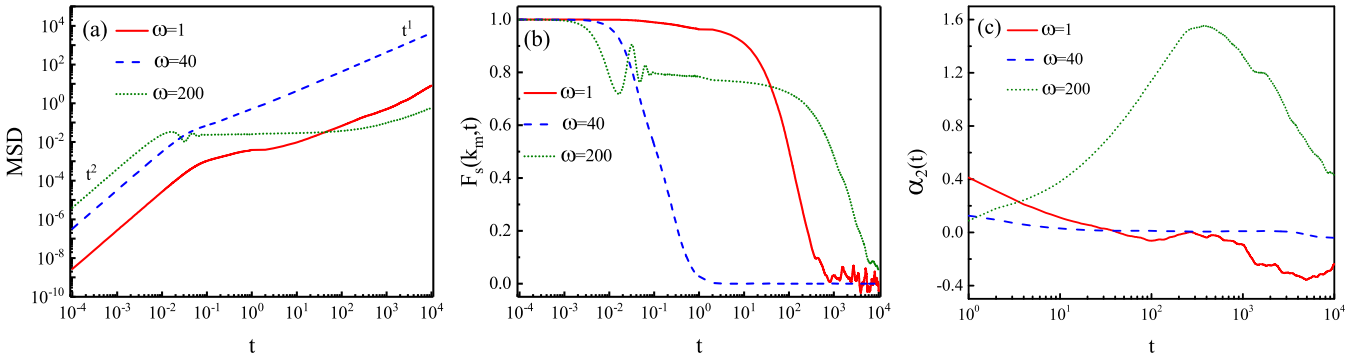

FIG. 10. (a) Mean-square displacement as a function of time t for different ω. (b) The self-intermediate scattering function of the majority A species as a function of t for different ω. (c) The non-Gaussian parameter as a function of time t for different different ω. The height of the peak in $\alpha_2(t)$ is an indicator for dynamical heterogeneity. A negative non-Gaussian parameter indicates the collective directional movement of particles in the system. The other parameters are $\tau_p = 0.01$ and $\tau_r = 0.1$.

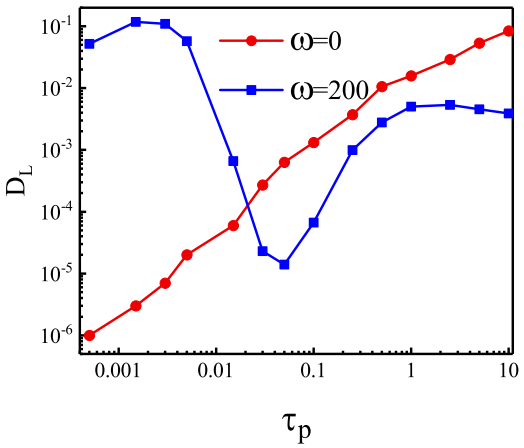

FIG. 11. The longtime diffusion coefficient D_L as a function of τ_p with ($\omega = 200$) and without ($\omega = 0$) chiral motion at $\tau_r = 0.01$. When ω is zero, we straightforwardly set $v_0 = 4$, without defining a specific spinning temperature.

low persistence regimes where $\tau^* < \tau_\omega$, particles experience random collisions with all neighboring particles. For intermediate persistence regimes defined by $\tau_\omega < \tau^* < 2\tau_\omega$, particles can complete a full circular or elliptical motion within their cages. Last, in high persistence regimes where $\tau^* \gg \tau_\omega$, the nearest-neighbor distance exhibits periodicity, suggesting that a particle collides, then drifts away, and repeats this process. In conclusion, the spinning period profoundly influences the glass dynamic behavior of the system.

In the preceding section, our focus was primarily on the two representative frequencies of $\omega = 10$ and 200 at $T_w = 4$, corresponding, respectively, to $v_0 = 4\sqrt{5}$ and 40. In these scenarios, self-propulsion significantly supersedes thermal fluctuations, thus allowing us to discount translational diffusion. Regardless, studying the influence of translational diffusion on the dynamics of glass-forming systems continues to be of great importance. Figure 12(a) presents the longtime diffusion coefficient D_L as a function of τ_r for varying D_0 at $\omega = 200$ and $\omega\tau_p = 0.2$. An intuitive result is observed: the longtime diffusion coefficient D_L increases in line with the growth of translational diffusion D_0. However, it is important to note that near the peak of the curves, D_L undergoes minimal changes irrespective of fluctuations in D_0. It can also be inferred that by modulating D_0, we can effectuate the transition from a liquid state to a glass state. For instance, when τ_r is kept constant at 1, a decrease in D_0 from 2.0 to 0 triggers a transition from the liquid state to the glass state. This transition can be described by the self-intermediate scattering function $F_s(k_m, t)$, as portrayed in Fig. 12(b). Furthermore, when the value of D_0 is adequately large, signifying the dominance of translational diffusion dynamics, D_L is almost independent of τ_r.

Finally, we briefly discuss the special collective behaviors of chiral active particles related to our system. As we know, in systems of chiral active particles, a nonequilibrium strongly hyperuniform fluid state [42,45] emerges with large local density fluctuations. However, in our system, even in the absence of noise and when the system is in a glassy state, a hyperuniform state was not observed. We propose two

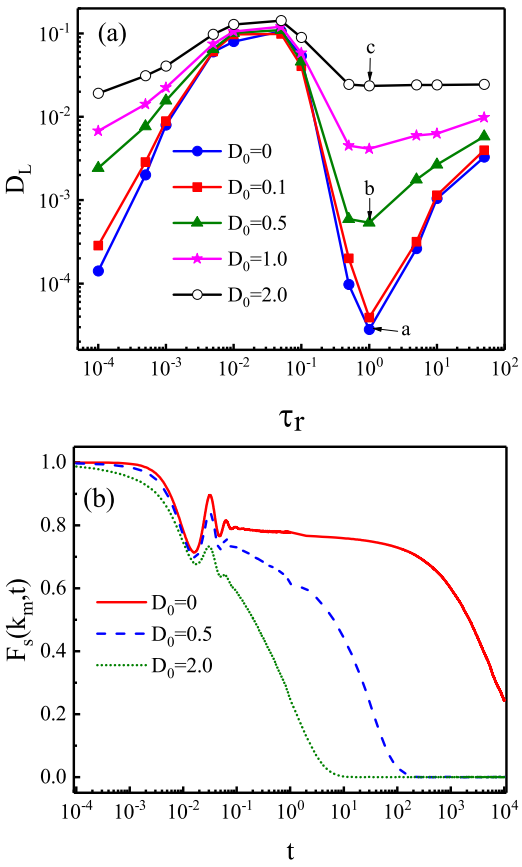

FIG. 12. (a) Longtime diffusion coefficient D_L as a function of τ_r for various values of D_0. (b) Self-intermediate scattering function of the majority A species as a function of time t for points a, b, and c as outlined in panel (a). The other parameters are maintained at $\omega = 200$ and $\omega\tau_p = 0.2$.

possible reasons for this: first, unlike systems in which hyperuniform states have previously been identified, our system is dense ($\rho = 1.2$), and the circular motion of the particles is constantly influenced by neighboring particles; second, the particles in our system vary in size, which is detrimental to the development of a hyperuniform state. In addition, in systems of chiral active particles, the chirality can induce the formation of dynamic clusters, which interrupt conventional motility-induced phase separation [46]. For our dense system, if the persistence time is short, chiral particles cannot form clusters; instead, they are trapped in effective confining potentials, leading the system to exhibit a glassy state. If the persistence time is intermediate, then chiral particles form very small clusters, and particles undergo prolonged periods of uninterrupted back-and-forth motion inside their cages. This can lead the system to transition from a glassy state to a liquid state. When the persistence time is long, chiral particles are able to form large clusters, with particle motion becoming more collective and vortexlike, resulting in the system being in a liquid state.

IV. CONCLUSION AND OUTLOOK

In the previous study [33], where rotational inertia was not considered, chiral glassy fluids displayed an extraordinarily intricate dynamical phenomenology characterized by a

nonmonotonic, reentrant, and significantly persistent regime. This complexity could be elucidated through the introduction of a hammering mechanism. In our current investigation, we delved into the dynamics of glass formation in chiral active particles when subjected to rotational inertia. We discovered that rotational inertia introduces an exponential memory to particle orientation, exerting a significant influence on the glassy dynamics. (1) For lower-frequency spinning (e.g., $\omega = 10$), the diffusion coefficient exhibits a peak function in relation to rotational inertia for shorter persistence times, while it shows a monotonic increase with rotational inertia for longer persistence times. (2) For high-frequency spinning (e.g., $\omega = 200$), the impact of rotational inertia on diffusion behavior becomes more pronounced, resulting in a nonmonotonic complex relationship between the diffusion coefficient and rotational inertia. In this regime, we observe phenomena such as two peaks and a valley in the $D_L - \tau_r$ curve for low persistence, allowing the diffusion coefficient to be adjusted between its apex and nadir values by altering rotational inertia. As the persistence time τ_p increases, both the first peak and the valley in the $D_L - \tau_r$ curve shift towards lower τ_r. Conversely, when the persistent time τ_p is substantially large, the peak and the valley vanish, rendering the diffusion coefficient seemingly indifferent to τ_r. Skillful adjustments to rotational inertia thus enable precise control over transitions between fluid and glassy states. Our research also unveiled the existence of an optimal spinning frequency at which the diffusion coefficient peaks. Furthermore, collective motion leads to an active state for low-frequency spinning and an absorbing state for high-frequency spinning.

Our findings provide substantial insights into understanding the glassy dynamics of chiral active matter influenced by rotational inertia. These insights hold promise for practical applications in future experimental designs aimed at observing such unique dynamics. Notably, these effects can be empirically corroborated in vibrated granular particles, assuming systematic alterations of mass and moment of inertia. Moreover, our system can manifest in various experimental frameworks, including macroscopic examinations of robotic or biological particles, or mesoscopic observations of self-propelled objects maneuvering in low-viscosity media like complex plasma. Remarkably, in dusty plasmas, particles exhibit inertia and engage in chiral dynamics within a magnetic field [47]. Additionally, extending our model to include obstacles may reveal how these obstacles influence the collective behavior of chiral particles. Future studies could intriguingly investigate the transitions of mechanisms, such as ratchets or gears, from the fluid to the glassy state and back to liquid within chiral fluids.

ACKNOWLEDGMENTS

This work was supported in part by the National Natural Science Foundation of China (Grants No. 12075090, No. 11975089, No. 12265017, No. 12247205), the Key-Area Research and Development Program of GuangDong Province (Grant No. 2019B030330001), the Guangdong basic and applied basic research foundation (Grants No. 2022A1515010449 and No. 2024A1515012575), and Yunnan Fundamental Research Projects (Grants No. 202101AS070018 and No. 202201AV070003).

[1] L. Berthier and G. Biroli, Rev. Mod. Phys. **83**, 587 (2011).
[2] K. Binder and W. Kob, *Glassy Materials and Disordered Solids: An Introduction to Their Statistical Mechanics* (World Scientific, Singapore, 2011).
[3] L. M. C. Janssen, J. Phys.: Condens. Matter **31**, 503002 (2019).
[4] B. R. Parry, I. V. Surovtsev, M. T. Cabeen, C. S. OaHern, E. R. Dufresne, and C. Jacobs-Wagner, Cell **156**, 183 (2014).
[5] T. E. Angelini, E. Hannezo, X. Trepat, M. Marquez, J. J. Fredberg, and D. A. Weitz, Proc. Natl. Acad. Sci. USA **108**, 4714 (2011).
[6] S. Grosser, J. Lippoldt, L. Oswald, M. Merkel, D. M. Sussman, F. Renner, P. Gottheil, E. W. Morawetz, T. Fuhs, X. Xie, S. Pawlizak, A. W. Fritsch, B. Wolf, L.-C. Horn, S. Briest, B. Aktas, M. L. Manning, and J. A. Kas, Phys. Rev. X **11**, 011033 (2021).
[7] N. Klongvessa, F. Ginot, C. Ybert, C. Cottin-Bizonne, and M. Leocmach, Phys. Rev. Lett. **123**, 248004 (2019).
[8] P. Arora, A. K. Sood, and R. Ganapathy, Phys. Rev. Lett. **128**, 178002 (2022).
[9] L. Berthier and J. Kurchan, Nat. Phys. **9**, 310 (2013).
[10] L. Berthier, Phys. Rev. Lett. **112**, 220602 (2014).
[11] E. Flenner, G. Szamel, and L. Berthier, Soft Matter **12**, 7136 (2016).
[12] L. Berthier, E. Flenner, and G. Szamel, New J. Phys. **19**, 125006 (2017).
[13] R. Ni, M. A. C. Stuart, and M. Dijkstra, Nat. Commun. **4**, 2704 (2013).
[14] S. K. Nandi, R. Mandal, P. J. Bhuyan, C. Dasgupta, M. Rao, and N. S. Gov, Proc. Natl. Acad. Sci. USA **115**, 7688 (2018).
[15] R. Mandal and P. Sollich, Phys. Rev. Lett. **125**, 218001 (2020).
[16] D. Bi, X. Yang, M. C. Marchetti, and M. L. Manning, Phys. Rev. X **6**, 021011 (2016).
[17] V. E. Debets, X. M. de Wit, and L. M. C. Janssen, Phys. Rev. Lett. **127**, 278002 (2021).
[18] V. E. Debets and L. M. C. Janssen, J. Chem. Phys. **157**, 224902 (2022).
[19] V. E. Debets and L. M. C. Janssen, Phys. Rev. Res. **4**, L042033 (2022).
[20] G. Janzen and L. M. C. Janssen, Phys. Rev. Res. **4**, L012038 (2022).
[21] G. Szamel, Phys. Rev. E **93**, 012603 (2016).
[22] G. Szamel, E. Flenner, and L. Berthier, Phys. Rev. E **91**, 062304 (2015).
[23] G. Szamel, J. Chem. Phys. **150**, 124901 (2019).
[24] A. Liluashvili, J. Onody, and T. Voigtmann, Phys. Rev. E **96**, 062608 (2017).
[25] M. Feng and Z. Hou, Soft Matter **13**, 4464 (2017).
[26] S. Henkes, Y. Fily, and M. C. Marchetti, Phys. Rev. E **84**, 040301(R) (2011).

[27] J. Reichert, S. Mandal, and T. Voigtmann, Phys. Rev. E **104**, 044608 (2021).
[28] R. Mandal, P. J. Bhuyan, P. Chaudhuri, C. Dasgupta, and M. Rao, Nat. Commun. **11**, 2581 (2020).
[29] C. Reichhardt and C. J. O. Reichhardt, Phys. Rev. E **100**, 012604 (2019).
[30] C. Hargus, J. M. Epstein, and K. K. Mandadapu, Phys. Rev. Lett. **127**, 178001 (2021).
[31] Y. Hosaka, S. Komura, and D. Andelman, Phys. Rev. E **103**, 042610 (2021).
[32] C. Bechinger, R. Di Leonardo, H. Löwen, C. Reichhardt, G. Volpe, and G. Volpe, Rev. Mod. Phys. **88**, 045006 (2016).
[33] V. E. Debets, H. Löwen, and L. M. C. Janssen, Phys. Rev. Lett. **130**, 058201 (2023).
[34] H. Löwen, J. Chem. Phys. **152**, 040901 (2020).
[35] L. Caprini and U. M. B. Marconi, J. Chem. Phys. **154**, 024902 (2021).
[36] A. R. Sprenger, S. Jahanshahi, A. V. Ivlev, and H. Löwen, Phys. Rev. E **103**, 042601 (2021).
[37] C. Scholz, S. Jahanshahi, A. Ldov, and H. Löwen, Nat. Commun. **9**, 5156 (2018).
[38] L. Caprini, R. K. Gupta, and H. Löwen, Phys. Chem. Chem. Phys. **24**, 24910 (2022).
[39] F. Weysser, A. M. Puertas, M. Fuchs, and T. Voigtmann, Phys. Rev. E **82**, 011504 (2010).
[40] P. Charbonneau, A. Ikeda, G. Parisi, and F. Zamponi, Proc. Natl. Acad. Sci. USA **109**, 13939 (2012).
[41] H. Ding, H. Jiang, and Z. Hou, Phys. Rev. E **95**, 052608 (2017).
[42] Q.-L. Lei, M. P. Ciamarra, and R. Ni, Sci. Adv. **5**, eaau7423 (2019).
[43] C. Donati, J. F. Douglas, W. Kob, S. J. Plimpton, P. H. Poole, and S. C. Glotzer, Phys. Rev. Lett. **80**, 2338 (1998).
[44] I. Tah, A. Mutneja, and S. Karmakar, ACS Omega **6**, 7229 (2021).
[45] B. Zhang and A. Snezhko, Phys. Rev. Lett. **128**, 218002 (2022).
[46] Z. Ma and R. Ni, J. Chem. Phys. **156**, 021102 (2022).
[47] H. Kählert, J. Carstensen, M. Bonitz, H. Löwen, F. Greiner, and A. Piel, Phys. Rev. Lett. **109**, 155003 (2012).